In-Situ X-ray Absorption Spectroscopy Study of Pt and Ru Chemistry during Methanol Electrooxidation†

William L. Holstein* and H. David Rosenfeld

Central Research & Development, E. I. duPont de Nemours, Inc., Wilmington, Delaware 19880-0262

Received: March 8, 2004; In Final Form: May 20, 2004

Methanol electrooxidation in a 0.5 M sulfuric acid electrolyte containing 1.0 M CH_3OH was studied on 30% Pt/carbon and 30% PtRu/carbon (Pt/Ru = 1:1) catalysts using X-ray absorption spectroscopy (XAS). Absorption by Pt and Ru was measured at constant photon energy in the near edge region during linear potential sweeps of 10−50 mV/s between 0.01 and 1.36 V vs rhe. The absorption results were used to follow Pt and Ru oxidation and reduction under transient conditions as well as to monitor Ru dissolution. Both catalysts exhibited higher activity for methanol oxidation at high potential following multiple potential cycles. Correlation of XAS data with the potential sweeps indicates that Pt catalysts lose activity at high potentials due to Pt oxidation. The addition of Ru to Pt accelerates the rate of methanol oxidation at all potentials. Ru is more readily oxidized than Pt, but unlike Pt, its oxidation does not result in a decrease in catalytic activity. PtRu/carbon catalysts underwent significant changes during potential cycling due to Ru loss. Similar current density vs potential results were obtained using the same PtRu/carbon catalyst at the same loading in a membrane electrode assembly half cell with only a Nafion (DuPont) solid electrolyte. The results are interpreted in terms of a bifunctional catalyst mechanism in which Pt surface sites serve to chemisorb and dissociate methanol to protons and carbon monoxide, while Ru surface sites activate water and accelerate the oxidation of the chemisorbed CO intermediate. PtRu/carbon catalysts maintain their activity at very high potentials, which is attributed to the ability of the added Ru to keep Pt present in a reduced state, a necessary requirement for methanol chemisorption and dissociation.

Introduction

Direct Methanol Fuel Cells. Recent advances in polymer electrolyte membrane (PEM) direct methanol fuel cell (DMFC) technology have raised interest in the use of DMFCs as power sources for portable electronic devices.[1] The scientific and engineering challenges have been summarized in several excellent reviews.[2−5]

The key materials impacting the performance of direct methanol fuel cells are the membrane and the electrocatalysts. The leading membrane material is DuPont Nafion (per fluoro sulfonic acid), which is commonly used in the form of a 7 mil (180 μm) membrane.[6] The membrane serves as a proton conductor and acts as a barrier for separating the fuel and the oxidant. Nafion is also added to the electrodes to enhance proton transport.

Pt black or Pt/carbon cathode catalysts are commonly used to catalyze the reduction of oxygen

$$O_2 + 4H^+ + 4e^- = 2H_2O \quad (1)$$

While Pt catalysts show appreciable activity for the electrooxidation of methanol

$$CH_3OH + H_2O = CO_2 + 6H^+ + 6e^- \quad (2)$$

bimetallic PtRu catalysts exhibit much higher activity, and they are used as anode catalysts in current direct methanol fuel cells either in the form of PtRu black or PtRu/carbon.[3,7] Electrocatalyst performance and lifetime are key development areas.

In-Situ X-ray Absorption Spectroscopy. X-ray absorption spectroscopy (XAS), encompassing both the study of the near edge region and the fine structure region at energies above the absorption edge, has proven invaluable in understanding the structure of catalysts.[8] For transition metals, absorption at the near edge region results from electronic transitions into the d band or bound states and it is a sensitive probe of a catalyst's oxidation state or d-band vacancies.[9,10] Most early in-situ X-ray absorption spectroscopy studies of heterogeneous catalytic reactions were carried out for gas-phase reactions, where photon absorption by reactants and products is minimal, using ionization detectors and serial data collection. Solid state detectors and parallel detection schemes based on dispersive optics have allowed for following temporal changes to catalysts under non steady-state conditions, but such experiments require highly uniform samples and are more complex to perform.[11−13]

The use of in-situ X-ray absorption spectroscopy to characterize electrocatalysts was pioneered by Boudart and co-workers,[14] who recognized the importance of in-situ measurements for elucidating the structure of catalysts during electrochemical reactions. The presence of strongly absorbing electrolytes and the need for counter electrodes, reference electrodes, and electrical contacts makes the in-situ study of electrocatalysts by XAS more complicated than the study of gas-phase heterogeneous catalysts. Boudart et al. designed a cell for transmission XAS that used a sulfuric acid electrolyte and Pt/carbon electrodes supported on hydrophobic porous carbon paper as windows on both sides of an electrochemical cell. The

† Part of the special issue "Michel Boudart Festschrift".

* Author to whom correspondence should be addressed. E-mail: William.L.Holstein@usa.dupont.com.

10.1021/jp048955h CCC: $30.25
Published on Web 07/22/2004

work in that study was aimed at understanding the behavior of catalysts for the electrochemical reduction of oxygen, where Boudart and his colleagues had observed a strong dependence of turnover rate on Pt particle size, concluding that Pt particles 3−4 nm in size would provide for the most effective utilization of expensive platinum.[15] This result, also noted by others,[16,17] has impacted the design of PEM fuel cell cathode catalysts, where effective utilization of Pt is crucial for minimizing product cost.

Since this early work, the use of XAS to study electrochemical phenomena has grown.[18,19] There are a handful of reports on the use of XAS for the in-situ study of Pt and PtRu methanol oxidation electrocatalysts.[20−24]

In this work, we discuss a simple XAS technique for qualitatively following the oxidation state of electrocatalysts under non-steady state conditions by using a fluorescence detector and serial data collection to monitor the absorption intensity as a function of time at a single X-ray energy. While the data that is collected is more limited than that which can be obtained by parallel collection schemes, it is sufficient for monitoring changes to the oxidation state of electrocatalysts that occur over periods of a few seconds. The technique has been applied to the study of changes in oxidation state and composition that occur for Pt/carbon and PtRu/carbon methanol oxidation catalysts during cyclic voltametry. A similar method has been used previously to study electrochemical oxidation of chemisorbed CO on highly dispersed Pt particles.[24]

Experimental Section

Sample Preparation. 30 wt % Pt/carbon catalysts and 30 wt % PtRu/carbon (1:1 Pt/Ru) catalysts from E-TEK were used. The catalyst support was Vulcan XC-72 with a BET surface area of 250 m^2/g. According to product specifications, the Pt surface area for the 30 wt % Pt/carbon catalyst was 88 m^2/g Pt, corresponding to a dispersion of about 35% and an average particle size of 3.2 nm, while the 30% PtRu/carbon catalyst had an average particle size estimated to be 2−4 nm. Transmission electron microscopy and X-ray absorption spectroscopy indicated that the Pt/carbon consisted of a reduced metal with a surface oxide, while the PtRu/carbon consisted of a mixture of reduced and oxidized materials. The Pt and PtRu were found to quickly and completely reduce to the metallic form at room temperature, both when exposed to a hydrogen atmosphere in a gaseous environment and when held at a potential of 0.0 V vs a reversible hydrogen electrode in 0.5 M H_2SO_4. A published study of similar E-TEK 20% PtRu/carbon (Pt/Ru = 1:1) catalysts following reduction in hydrogen at 300 °C showed them to consist of face-centered cubic solid-solution PtRu alloy nanocrystals with uniform composition.[25]

Electrode layers were prepared on 1.0 cm-wide strips of porous Toray carbon paper with an average thickness of 0.17 mm and an average density of 0.49 g/cm^3. Each strip was individually tared. A solution containing 0.45 wt % Nafion and 2.37 wt % Pt/carbon or PtRu/carbon powder in water was prepared and stirred at high speed for 30 min. An eyedropper was used to transfer a controlled amount of the stirred solution onto a 1.5 cm length of a 5 cm-long carbon paper strip. The wet carbon strip was set on aluminum foil and allowed to dry in air. It was then heated to 100 °C in a vacuum oven for 30 min. Following removal from the oven and cooling, the strips were again tared to determine the added weight from the Pt/carbon + Nafion coating. The weights of the loadings corresponded to the deposition of 4.5 ± 0.3 mg total metal, or a metal loading of 0.30 ± 0.02 mg Pt (or PtRu)/cm^2. The final catalyst consisted of a moderately uniform coating of carbon-supported metal catalyst bonded by Nafion on one surface of the porous carbon paper. In addition to promoting adhesion of the catalyst powder to the carbon strip, the Nafion can serve as a proton conductor.

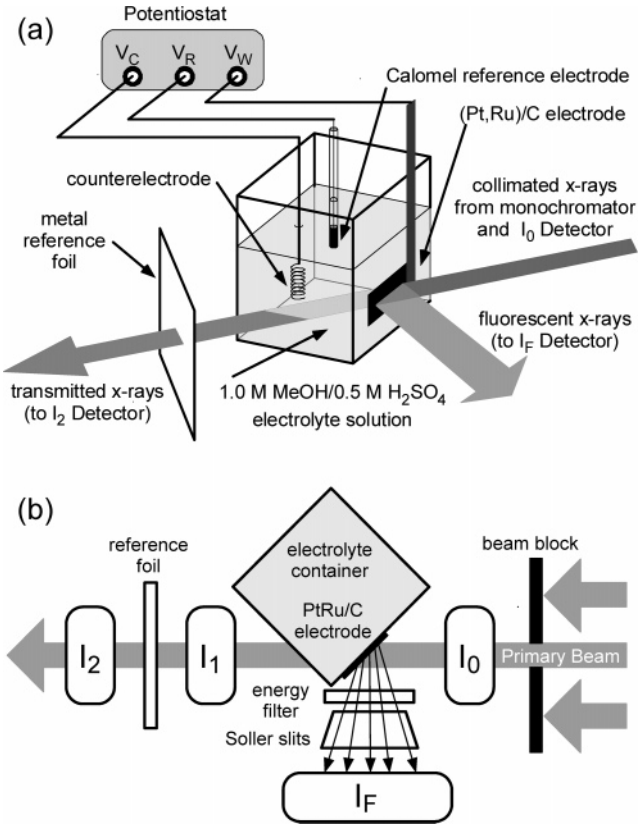

Figure 1. (a) Schematic diagram of experimental setup showing electrochemical cell and potentiostat (V_W: working electrode, V_C: counter electrode, V_R: reference electrode). (b) Top-down view showing paths of X-rays and locations of sample, reference sample, gas ionization detectors (I_0, I_1, and I_2) and the Lytel fluorescence detector (which incorporates the Soller slits, energy filter, and I_F detector).

Electrochemical Cell Set-Up. An in-situ electrochemical cell was designed for use in combination with X-ray absorption spectroscopy. A hole was cut in one side of a 125 cm^3 polyolefin bottle (Figure 1a). The carbon paper strip containing the catalyst sample was placed on the outside of the bottle and located over the hole that had been cut into the bottle. The side of the strip containing the electrode layer faced the inside of the bottle.

Two strips of polycrystalline graphite (one on each side of the sample) were used to make electrical contact to the carbon paper. (Only one of the two graphite strips is shown in the Figure 1a.) The porous carbon paper and graphite contact rods were sealed with Kapton (DuPont) tape. Electrical contact was made to the graphite strips using copper-coated duck-bill connectors. Good electrical contact between the carbon paper and the graphite strips, as well as between the graphite strips and the copper-coated connectors, was assured by measuring the electrical resistance through the connector−graphite strip−carbon paper strip−graphite strip−connector circuit prior to the start of the experiment.

For the experiments described here, the electrochemical cell was filled with a solution of 1.0 M CH_3OH in 0.5 M H_2SO_4. The potential of the working electrode containing the Pt/carbon or PtRu/carbon catalyst was controlled with a potentiostat. A coiled platinum wire was used as a counter electrode, and a saturated calomel electrode was used as the reference electrode.

All experiments were carried out at an ambient temperature of about 25 °C. All of the equipment, including the potentiostat, was located within the experimental hutch providing protection from stray X-rays. The potentiostat was operated from within the hutch, while the X-ray equipment was operated from a computer located outside the hutch.

XAS Set-Up. A top-down view of the experimental layout illustrating the locations of the electrochemical cell and the X-ray detectors is shown in Figure 1b. A bending magnet in combination with a 30% detuned quartz crystal monochromator was used as the source of monochromatic, collimated X-rays, which enter from the right in the diagram. The resulting beam was passed through a physical aperture to reduce the cross sectional area to 5 mm wide × 1 mm high. The intensity of the incoming beam (I_0) was measured with a gas ionization detector containing inert gases selected to allow for about 80% transmission.

The electrochemical cell was placed in the path of an X-ray beam shortly downstream of the I_0 detector. The vessel was oriented at a 45 degree angle to the beam. The position of the vessel was adjusted to ensure that the beam illuminated the area of the sample located over the hole, creating an illumination area of about 7 × 1 mm. The primary beam then passed through the vessel, a gas ionization detector (I_1), a reference film, and a final ionization detector (I_2). Both the I_1 and I_2 detectors were filled with gases designed to allow for about 60% beam transmission. Data measured by the I_1 and I_2 detectors were used to measure the absorption by the reference film (absorption $\propto \ln(I_1/I_2)$), which in turn was used to calibrate the beam energy from the known location of the absorption edge.

Complete absorption spectra of the near edge and extended fine structure regions were measured for the Pt, PtO_2, $PtO_2(H_2O)_x$, Ru, RuO_2, and $RuO_2(H_2O)_x$ reference standards in transmission mode by removing the electrochemical cell and using the I_1 and I_0 detectors. Absorption is proportional to $\ln(I_0/I_1)$).

Absorption by the in-situ samples was measured with a Lytel fluorescence detector located at a 45 degree angle to the sample and at a 90 degree angle to the incoming beam (Figure 1b). Gallium and molybdenum filters were used during the study of the Pt-L_{III} and Ru K edges, respectively. The filters reduce the intensity of elastically scattered radiation reaching the detector, while having minimal impact on the desired flourescence radiation. Reported absorption data reflects the ratio of the measured X-ray fluorescence intensity to the intensity of the primary beam (absorption $\propto I_F/I_0$).

In-Situ XAS Experiments. X-ray absorption studies of Pt and Ru were carried out during linear potential sweeps. The current density J is based on the geometric area, and the potential E is reported vs a reversible hydrogen electrode in the same electrolyte (rhe). The electrochemical cell was set in place and aligned with respect to the incoming beam and fluorescence detector. The potentiostat was turned on and the applied potential was set at 0.76 V for several minutes prior to the start of cyclic voltametry experiments.

Cyclic voltametry experiments were initiated at 0.76 V. For the experiments described here, scan rates of 10 and 50 mV/s were used. The voltage was first increased to 1.36 V, then decreased to 0.01 V, and then cycled between 0.01 and 1.36 V. The first full cycle is defined as the period of time starting when the sample first reached 0.01 V to the time when it returned to this potential. Subsequent cycles are defined in a like manner. The potentiostat was run from within the hutch, and—due to the need to seal the hutch and open the window for the X-ray beam—a short period of time elapsed between starting the potential cycling and the start of XAS data collection. Rather than taking full scans of the near edge region, XAS data were collected at constant X-ray energy, as elaborated further below. Absorption measurements were carried out using a count time of 0.5 s for the potential scans at 50 mV/s and 2 s for the potential scans at 10 mV/s. These count times correspond to potential changes of 25 mV and 20 mV, respectively.

Since absorption at only one absorption edge (Pt-L_{III} or Ru K) could be studied at a time, the time-dependent absorption results presented in this study were compiled on different identically prepared and mounted samples that underwent the identical potential cycling protocol. Additional potential cycling studies were carried out on samples in the absence of concurrent study by X-ray absorption. The potential cycling studies for repeat runs exhibited only minor differences.

Membrane Electrode Assembly Half-Cell Measurements. In addition to the extensive potential cycling studies carried out in a liquid electrolyte, additional studies were carried out on a 5 cm^2 fuel cell membrane electrode assembly in order to relate the liquid electrolyte experiments to actual DMFC operating conditions, in which only a solid electrolyte is present. The E-TEK 30% PtRu/carbon anode catalyst was mixed with a Nafion solution and coated onto a Toray porous carbon paper diffusion backing layer. The average metal loading was 0.30 mg/cm^2. A second electrode was prepared in a similar manner with a Pt black electrocatalyst. The two electrodes were placed on opposite sides of a 180 μm-thick Nafion membrane. The resulting assembly is essentially identical to that which is used for single cell testing of membrane electrode assemblies (MEAs) for direct methanol fuel cells, although metal loadings for actual direct methanol fuel cells are typically about an order of magnitude higher.

Results

Reference Samples. Transmission X-ray absorption spectra at the Ru K edge in both near edge (XANES) and extended fine structure (EXAFS) regions were recorded for a ruthenium metal film, RuO_2 powder (Alfa Aesar), and hydrous RuO_2 powder (Alfa Aesar; $H_2O/RuO_2 = 2.6$). Near edge spectra, following background correction and normalization, are shown in Figure 2a for Ru and RuO_2. As expected, the absorption edge for RuO_2 is shifted to higher energies. The spectrum for hydrous RuO_2 in the edge region differed only slightly from that for RuO_2. The results are consistent with those reported in previous studies.[23,26]

Transmission X-ray absorption spectra at the Pt-L_{III} edge were recorded for platinum metal foil, PtO_2 powder (Alfa Aesar), and hydrous PtO_2 powder (Alfa Aesar, $H_2O/PtO_2 = 2.2$). Normalized absorption spectra following background correction are shown in Figure 2b for Pt and PtO_2. Transmission X-ray spectra for Pt and PtO_2 at the L_{III} edge have previously been reported by Boudart and co-workers,[14] and the near edge spectra measured in this work for these two materials appeared similar to those reported in that earlier work. The near edge spectra of hydrous PtO_2 differed only slightly from that for PtO_2 in the edge region.

Comparison of the spectra for metallic and oxidized Ru indicates significantly higher absorption intensity for the oxidized form of Ru at energies between 22.140 and 22.152 keV (Figure 2a). Thus, monitoring the absorption at fixed photon energy between 22.140 and 22.152 keV can be used to qualitatively monitor the oxidation state of Ru. A photon energy of 22.145 keV was selected to differentiate between oxidized

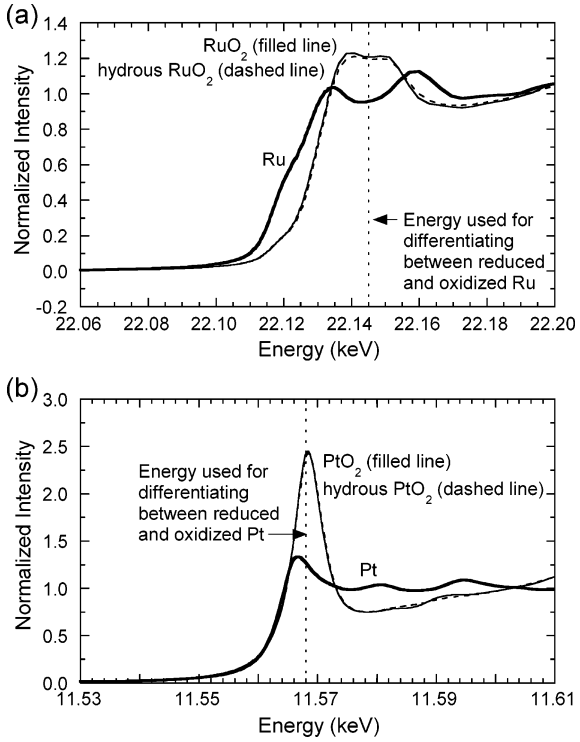

Figure 2. X-ray absorption edge spectra: (a) Pt-L_{III} edge for Pt foil, PtO_2 powder, and hydrous PtO_x powder ($H_2O/PtO_2 = 2.2$), and (b) the Ru K edge for a Ru film, RuO_2, and hydrous RuO_2 powder ($H_2O/RuO_2 = 2.6$). The spectra for the oxides and hydrous oxides overlap over much of the energy range. Photon energies used for differentiating between the oxidized and reduced forms of Pt and Ru are noted by dashed lines.

and reduced Ru as shown in the figure. A similar enhancement in absorption by PtO_2 and hydrated PtO_2 vs Pt is observed between energies of 11.566 and 11.572 keV, and a photon energy of 11.568 keV was chosen to differentiate between reduced and oxidized forms of platinum (Figure 2b). The spectra in Figures 2a and 2b show the limiting cases for fully reduced Pt and Ru and the +4 oxidation state oxides of the same elements. Gas-phase chemisorption studies of oxygen onto highly dispersed Pt particles, which result in a lower average oxidation state for Pt, leads to near edge features intermediate between those of Pt and PtO_2.[27−29] These white line features for Pt result from 2p electron transitions into d-band vacancies. In-situ XAS electrochemical studies suggest a linear relationship between the intensity of the white line absorption and the degree of oxidation.[30]

In-Situ Electrochemistry. Cyclic voltametry scans at 10 mV/s for the Pt/carbon electrode in 1.0 M MeOH + 0.5 M H_2SO_4 are shown in Figure 3. At this scan rate, each cycle lasts 270 s. For clarity, current density is plotted as a function of potential only for cycles 2, 4, 6, 12, and 22. Intermediate cycles evolved in a manner consistent with the results shown in the figure.

All of the cycles exhibit a similar shape. The current from methanol oxidation becomes apparent as the potential rises above 0.45 V. The current density increases as the potential increases and reaches a maximum at potentials ranging from 1.08 V for the second cycle to 1.20 V for the twenty-second cycle. It then drops off quickly with further increases in potential, reaching a minimum, and then increases again as the voltage is further increased to the highest potential of 1.36 V. As the potential is decreased, the rate drops sharply, reaching

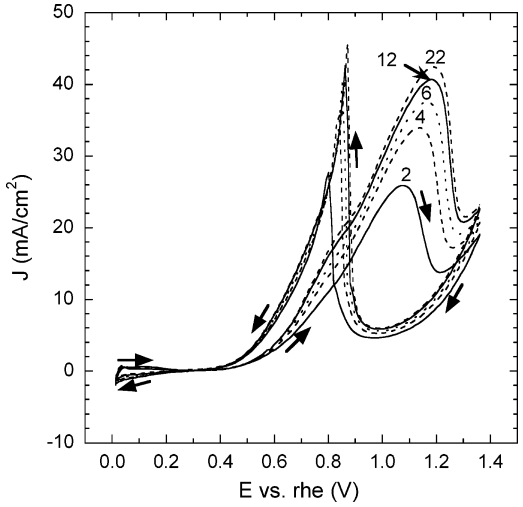

Figure 3. Current density J vs potential E for 30% Pt/carbon cycled between potentials of 0.01 and 1.36 V vs rhe at 10 mV/s. Results for cycles 2, 4, 6, 12, and 22 are shown. Arrows show the progression of the second cycle.

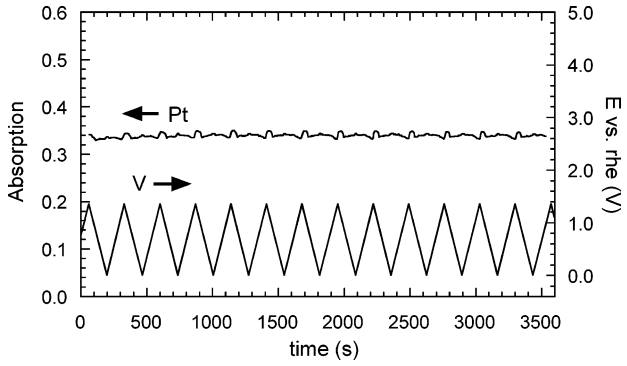

Figure 4. Absorption at the Pt-L_{III} edge and potential vs time during potential cycling of 30% Pt/carbon between potential of between 0.01 and 1.36 V vs rhe at 10 mV/s.

a minimum at a potential of about 0.98 V and then increases sharply with further decreases in potential. It reaches a sharp maximum on the decreasing voltage half of the cycle at potentials ranging from 0.80 V for the second cycle to 0.87 V for the twenty-second cycle, and then decreases with further decreases in potential.

The shapes of the current density vs potential curves are similar for all of the cycles. However, the locations of the maxima and minima in current density shift. In particular, the current density maxima for both the increasing and decreasing potential parts of the cycles shift to higher potentials and current densities during the first few cycles. These changes become less significant after a handful of cycles, and after about 12 cycles, further changes are very small.

X-ray absorption by Pt at a photon energy of 11.568 V was measured as a function of time during potential cycling at 10 mV/s for 22 cycles. Results for the first 12 cycles are shown in Figure 4. Figure 5a shows the absorption values for the first and second cycle and Figure 5b for the tenth and eleventh cycle. During both initial and latter cycles, the decrease in rate of methanol oxidation correlates with an increase in platinum absorption due to oxidation. For the early cycles, the onset of Pt oxidation becomes noticeable at about 1.27 V on the increasing potential half of the cycle and the onset of reduction at about 0.72 V on the decreasing potential half of the cycle (Figure 5a). For the latter cycles, Pt oxidation and reduction occur at slightly higher potentials (Figure 5b).

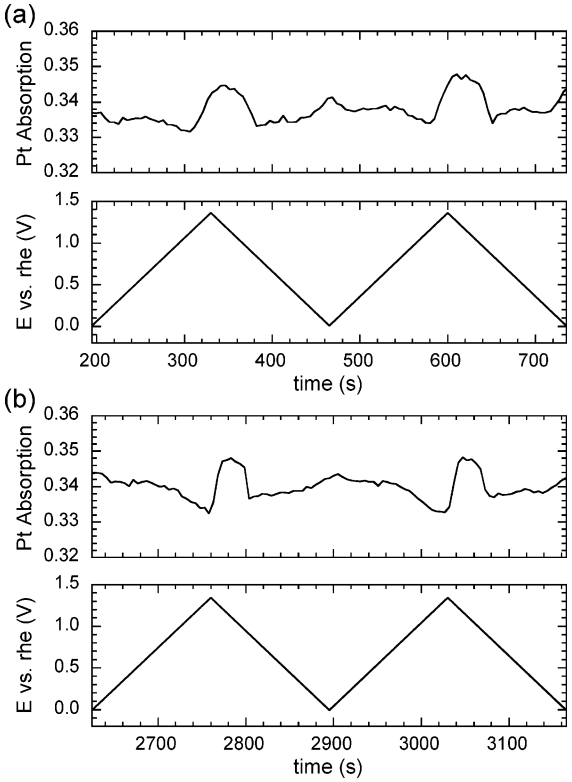

Figure 5. Absorption at the Pt-L_{III} edge vs time during CV cycling at 10 mV/s: (a) cycles 1 and 2, and (b) cycles 10 and 11.

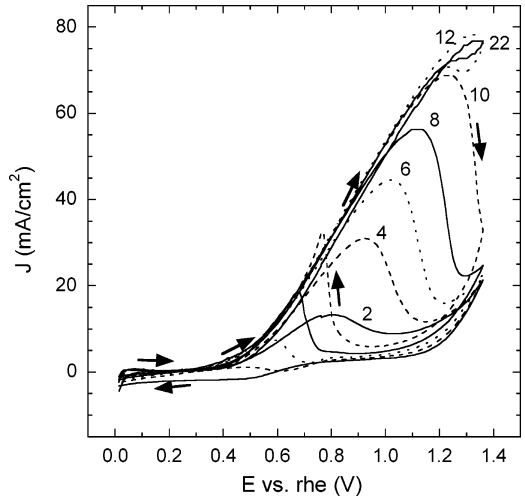

Figure 6. Current density *J* vs potential *E* for 30% PtRu/carbon cycled between potentials of 0.01 and 1.36 V vs rhe at 10 mV/s. Results for cycles 2, 4, 6, 8, 10, 12, and 22 are shown. Arrows show the progression of the tenth cycle.

Cyclic voltametry results for the PtRu/carbon electrode cycled in 1.0 M MeOH + 0.5 M H_2SO_4 at 10 mV/s are shown in Figure 6. The onset of methanol oxidation occurs at about 0.40 V. There are strong changes in the potential cycles over time. The early cycles exhibit a low maximum current density at moderate potentials for the increasing potential half of the cycle and there is no maximum in current density during the decreasing potential half of the cycles. As the number of cycles increases, the potential for which the current density peaks during the increasing potential half of the cycle shifts to higher values and the maximum current density increases greatly. Once the rate of methanol oxidation has peaked and dropped off, the rate is not restored until the potential has been decreased to well below the peak potential of 1.37 V. Indeed, no maximum in current

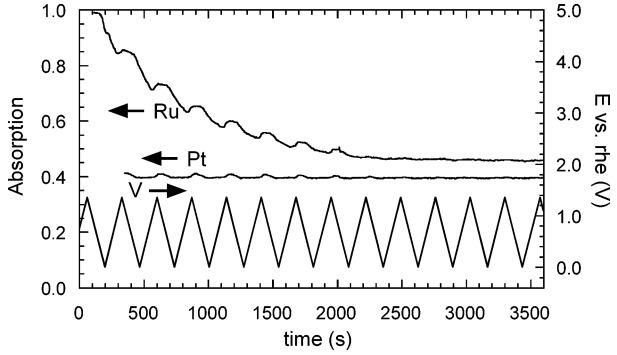

Figure 7. Absorption at the Pt-L_{III} and Ru K edges vs time during potential cycling of 30% PtRu/carbon between potentials of 0.01 and 1.36 V vs rhe at 10 mV/s.

density is observed during the decreasing potential part of the cycle for the first few cycles. By the sixth cycle, the current density maximum is located at a potential of about 0.77 V. Significant changes are observed between the sixth and twelfth cycles. The maximum in the decreasing potential part of the cycle moves to higher voltages and the maximum current density increases. For cycles greater than the twelfth cycle, very little hysteresis is observed.

X-ray absorption by Pt and Ru at photon energies of 11.568 and 22.145 keV was measured while cycling the potential between 0.01 and 1.36 V for 22 cycles. Results are plotted as a function of time in Figure 7 over the course of the first 12 cycles. Figure 8a shows the Pt and Ru absorption for the third and fourth cycles and Figure 8b shows the absorption for the eleventh and twelfth cycles.

The intensity of the Ru absorption decreases noticeably during the first twelve cycles. During this period of time, over half of the ruthenium is leached from the sample. Ru loss was confirmed at the completion of the voltage cycling by full Pt and Ru absorption scans of the near edge region and, following completion of the experiment and removal of the sample, by transmission electron microscopy and X-ray microanalysis.

No measurable decrease in the intensity of the ruthenium absorption was noted when the sample was held continuously under reducing conditions (a potential of 0.01 V) or oxidizing conditions (a potential of 1.36 V). Rather, ruthenium leaching resulted from cycling the sample between oxidizing and reducing potentials.

Oscillations in Ru intensity with a period corresponding to the 270 s cycle are superimposed on top of the continuously decreasing Ru absorption due to dissolution in Figure 7. These oscillations correspond to an increase in absorption due to Ru oxidation at the higher potentials and a decrease in absorption due to Ru reduction at the lower potentials.

The intensity of the Pt absorption for the PtRu/carbon sample undergoes oscillations for the initial cycles but not for the latter cycles. The intensity of the Pt signal at 0.01 V remains constant over the course of the 12 cycles, indicating that during the latter cycles Pt remains fully reduced, even at the higher potentials. The behavior of Pt in the PtRu/carbon catalyst during the latter cycles is notably different from that for Pt/carbon (Figures 4 and 5b), where the Pt was partially oxidized at the higher potentials.

The experiments described above were carried out at a scan rate of 10 mV/s. Additional experiments were carried out at faster and slower scan rates. Current density vs potential results for the PtRu/carbon catalyst at a scan rate of 50 mV/s are shown in Figure 9. Here the cycle time is 54 s. The curves have features similar to those recorded at 10 mV/s in Figure 6. Both scan

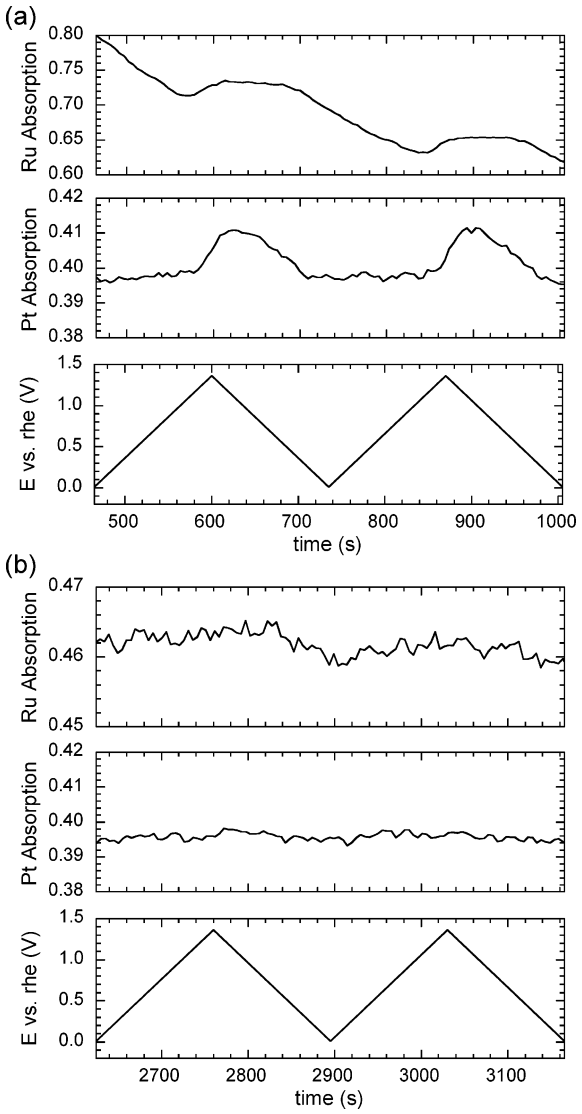

Figure 8. Absorption vs time at the Pt-L_{III} and Ru K edges during potential cycling at 10 mV/s: (a) cycles 3 and 4 and (b) cycles 11 and 12.

rates result in peak current densities of about 75 mA/cm^2 at the maximum potential of 1.36 V after numerous cycles. The features in the current density vs potential plots require about twice as many cycles to develop for the higher scan rate. As expected, features at potentials less than 0.4 V commonly associated with hydrogen chemisorption and double layer charging are more evident at the higher scan rate since comparable charges flow during a shorter period of time.

The intensity of Pt and Ru absorption at photon energies of 11.568 and 22.145 keV, respectively, are plotted vs time in Figure 10 for the first 36 full cycles. Detailed results are shown for the second and third cycles in Figure 11a and for the seventeenth and eighteenth cycles in Figure 11b. Qualitatively, the results look similar to those recorded at a scan rate of 10 mV/s (Figures 7 and 8). The more rapid cycling helps to differentiate the change in the Ru absorption resulting from oxidation−reduction from that due to ruthenium dissolution.

MEA Half-Cell Measurements. Experiments with anode catalysts in membrane electrode assembly (MEA) half cells were carried out in potentiostatic mode at 25 °C by flowing a 1.0 M MeOH solution at 10 mL/min through a serpentine channel flowfield overlaying the working electrode (anode). The methanol flow rate corresponded to a methanol conversion of less

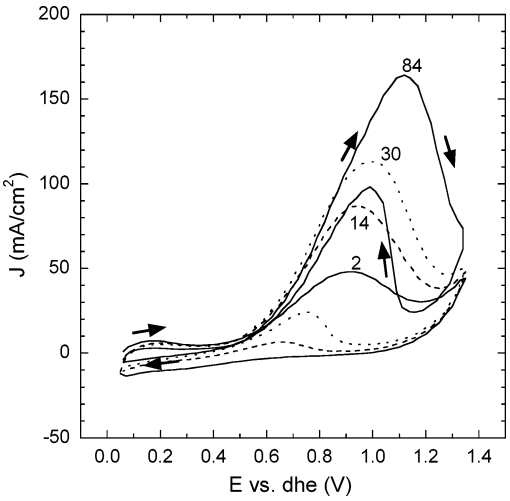

Figure 9. Current density J vs potential E for 30% PtRu/carbon cycled between potentials of 0.01 and 1.36 V vs rhe at 50 mV/s. Results for cycles 2, 6, 10, 14, 18, and 22 are shown. The arrows show the progression of the fourteenth cycle.

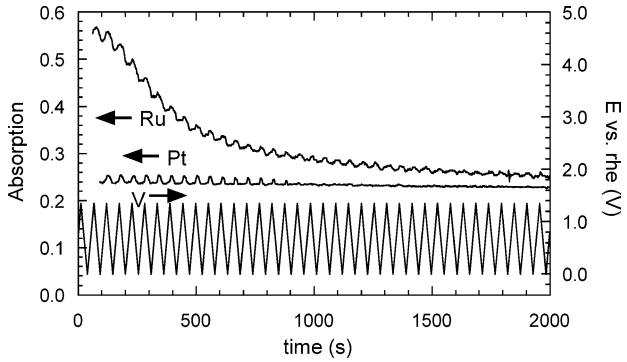

Figure 10. Absorption at the Pt-L_{III} and Ru K edges vs time during CV cycling between potentials of 0.01 and 1.36 V vs rhe at 50 mV/s.

than 1% at the highest current densities, and the working electrode chamber can be treated as a differential reactor. Simultaneously, hydrogen was passed through the counter electrode (cathode) flowfield on the opposite side of the Nafion membrane at 100 sccm. In potentiostatic mode, the reaction on the counter electrode is

$$2H^+ + 2e^- = H_2(g) \qquad (3)$$

This reaction occurs on the counter electrode with negligible overpotential, and the electrode serves a dual role as a dynamic hydrogen reference electrode (dhe).[31]

The potentials reported for the MEA experiment reflect the measured voltage across the cell. They were not corrected for IR losses across the cell, which were estimated to be about 30 mV at the highest current densities. Thus, the actual potentials at the working electrode are slightly lower than the uncorrected values shown in Figure 12.

The PtRu/carbon working electrode was cycled between potentials of 0.05 and 1.35 V vs dhe. Current density vs potential results are shown in Figure 12. Data are shown for cycles 4, 18, 30, and 84. The changes in current density vs potential with increasing cycle number are similar to those in Figure 9 for the same PtRu/carbon catalyst cycled at the same rate in 0.5 M H_2SO_4. However, the changes occur more rapidly in the liquid electrolyte than for the solid electrolyte. The results indicate that Ru dissolution is occurring in the presence of the solid electrolyte as well as for the liquid electrolyte. Subsequent

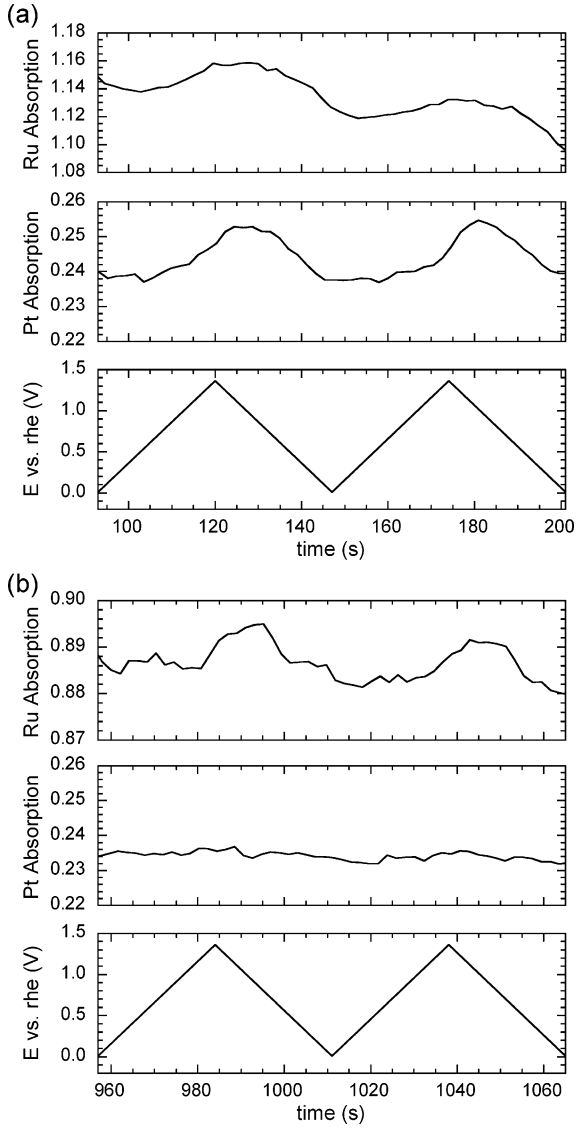

Figure 11. Absorption vs time at the Pt-L_{III} and Ru K edges during potential cycling at 50 mV/s: (a) cycles 2 and 3, and (b) cycles 17 and 18.

transmission electron microscopy/X-ray microanalysis of the working electrode catalyst confirmed a significant loss of Ru from the PtRu/carbon catalyst, as was the case for the liquid electrolyte.

Discussion

XAS Scans at Constant Photon Energy. The technique of recording X-ray absorption data at constant photon energy is suitable for studying rapid changes in oxidation state under conditions where the material being studied exhibits a significant change in absorption between the oxidized and reduced state. Small changes in metal loading can also be monitored. The experimental limitation for studying both phenomena is the signal/noise ratio, which is dependent on a wide range of factors, including the intensity of the incoming beam, the amount of material present, the fluorescence yield, and noise from the detector. In this study, count times as short as 0.5 s were found to be suitable for studying changes in absorption intensity of a few percent. While such constant photon energy measurements cannot provide the full depth of information available from full scans of the near edge and extended fine structure regions, when used in concert with such measurements, the technique allows

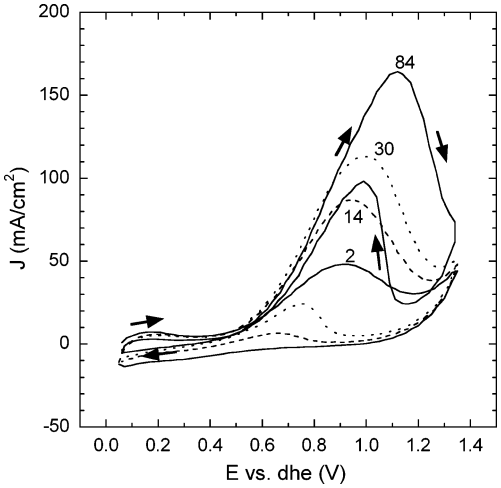

Figure 12. Current density *J* vs potential *E* for potential cycling of 30% PtRu/carbon anode in a membrane electrode assembly half cell between potentials of 0.05 and 1.35 V vs dhe at 50 mV/s. Results for cycles 2, 14, 30, and 84 are shown. Arrows show the progression of the eighty-fourth cycle.

for the easy study of transient phenomena where significant changes occur over the course of time intervals as short as a few seconds.

Turnover Rates. Due to the short times involved in cyclic voltametry, it is informative to consider the turnover rate, defined as the number of methanol molecules oxidized per catalyst site per second,[32] and the number of catalyst turnovers during the course of a full voltage cycle. In order for the reaction to be considered a catalytic reaction, the number of catalyst turnovers per cycle must significantly exceed unity.

A total of six electrons are generated for each methanol molecule that is oxidized (eq 2). On the basis of a Pt loading of 0.3 mg Pt/cm^2 and a dispersion of 35%, a current density of 10 mA/cm^2 corresponds to a turnover rate for methanol oxidation of 0.032/s. The peak current density of about 45 mA/cm^2 for the 10 mV/s scan for Pt/carbon in Figure 3 corresponds to a peak turnover rate of about 0.144/s. Integrating the current densities over the course of an entire cycle—which cancels out any current flows from metal oxidation and reduction—indicates that 6.5 and 9.8 methanol molecules were oxidized per Pt surface atom during the second and twenty-second cycles, respectively.

In the case of the PtRu/carbon catalysts, the number of Pt surface sites is known less precisely and most likely changes as ruthenium is leached from the sample. The 1:1 Pt/Ru ratio and the total metal loading of 0.30 mg/cm^2 yield a Pt loading of about 0.20 mg Pt/cm^2. Assuming, as was the case for Pt/carbon, that about 35% of the Pt atoms are on the surface and defining the turnover rate as the rate per Pt surface atom, a current density of 10 mA/cm^2 corresponds to a turnover rate of 0.048/s and the peak current density of 75 mA/cm^2 for scans recorded at both 10 mV/s and 50 mV/s correspond to a turnover rate of 0.36/s. Integrating the current densities over the course of an entire cycle at 10 mV/s indicates that 6.0 and 35.7 methanol molecules were converted per Pt surface atom during the second and twenty-second cycles, respectively.

The above calculations for both Pt/carbon and PtRu/carbon catalysts indicate that the methanol oxidation phenomena being studied are the result of a catalytic reaction rather than a combination of stoichiometric reactions induced by the voltage cycling, as is, for example, the case when voltage cycling is used for carbon monoxide stripping measurements of catalyst surface area.[31,33]

Methanol Electrooxidation Reaction Mechanism. The electrochemical oxidation of methanol is a complex reaction that requires the activation of both methanol and water. Several reviews summarize earlier work.[3,34−39] There is general agreement on the overall framework of the reaction mechanism, which has evolved from the bifunctional mechanism first proposed by Watanabe et al. for platinum alloys,[40,41] but there are many differing views on the details.

On unalloyed Pt, methanol is stripped of its hydrogen atoms through a series of elementary steps. One conceptualization of this mechanism can be written as

$$CH_3OH + Pt_s = Pt_s{-}CH_2OH + H^+ + e^- \quad (4)$$

$$Pt_s{-}CH_2OH = Pt_s{-}CHOH + H^+ + e^- \quad (5)$$

$$Pt_s{-}CHOH = Pt_s{-}COH + H^+ + e^- \quad (6)$$

$$Pt_s{-}COH = Pt_s{-}CO + H^+ + e^- \quad (7)$$

where Pt_s represents a Pt surface atom. Most evidence indicates that these steps are rapid, leading to a Pt surface that is largely covered with chemisorbed carbon monoxide, or possibly, a chemisorbed COH moiety. Water is activated through the step

$$Pt_s + H_2O = Pt_s{-}OH + H^+ + e^- \quad (8)$$

forming chemisorbed hydroxyl. Finally, the chemisorbed carbon monoxide and hydroxyl react to form carbon dioxide and free surface sites for the next catalytic cycle

$$Pt_s{-}CO + Pt_s{-}OH = 2Pt_s + CO_2 + H^+ + e^- \quad (9)$$

There are several slight variations to the theme, but general agreement that the most abundant surface intermediate is chemisorbed carbon monoxide (or in some views, a chemisorbed COH species) and the rate-determining step is the reaction of the chemisorbed CO with a hydroxyl group (Step (7)).

Bimetallic metal alloy catalysts provide an alternate pathway for activation of water and the oxidation of chemisorbed CO. In the case of a platinum−ruthenium bimetallic alloy, Steps (4)−(7) take place on Pt sites on the alloy surface, Pt_s, leading to the formation of $Pt_s{-}CO$. The presence of ruthenium atoms on the surface makes possible the activation of water through the alternate step

$$Ru_s + H_2O = Ru_s{-}OH + H^+ + e^- \quad (10)$$

The rate-determining step is the reaction of the chemisorbed CO and hydroxyl species

$$Ru_s{-}OH + Pt_s{-}CO = Ru_s + Pt_s + CO_2 + H^+ + e^- \quad (11)$$

On the alloy surface, methanol and water dissociation can take place on different sites. Methanol has been shown not to chemisorb on ruthenium.[42] Thus, water activation is not hindered for the PtRu alloy, even if the Pt sites are covered with strongly bound carbon monoxide.

The work in this study provides some additional clues regarding the mechanism. In the case of the Pt/carbon catalyst, the catalyst activity decreases under conditions leading to Pt oxidation. The loss of activity is attributed to the loss of Pt sites for methanol chemisorption. It is interesting to note that following Pt reduction during the downward voltage sweep, the activity of the Pt/carbon catalyst is comparable to or even higher than that of the PtRu/carbon catalyst (Figures 3 and 6). It is tempting to speculate that the comparable activity is due to a high rate of methanol oxidation on an unalloyed Pt surface that, following reduction, is initially covered with hydroxyls rather than chemisorbed CO. The enhanced current density for the decreasing voltage half of the cycle vs that for the increasing potential half in Figure 3 corresponds to the reaction of less than a monolayer of oxygen with methanol.

The activity of the PtRu/carbon catalyst, by contrast to that for Pt/carbon, is comparable during the increasing potential and decreasing potential halves of each cycle for potentials where Pt is present in a reduced state (Figure 6). The similarity in current densities for PtRu/carbon during upward and downward voltage sweeps during latter cycles is explained by considering that the rate of methanol oxidation during the increasing potential half of the cycle is not limited by the presence of chemisorbed CO on Pt, as is the case for Pt/carbon.

One of the main areas of contention regarding the catalytic mechanism is whether the accelerated rate for PtRu vs Pt is due to the presence of a PtRu alloy or distinct Pt and Ru phases. High specific activity has been found for PtRu catalysts prepared by a wide variety of methods, including the following: single-phase bulk PtRu alloys,[43] ruthenium-decorated platinum surfaces,[40,44] colloidal PtRu black,[27] and carbon-supported PtRu particles.[7,45] The work in this study indicates that high activity requires only that Pt and Ru sites be present in close proximity. Full spectra of the edge region indicate that both Pt and Ru are present in the reduced state at low potentials. As the anode potential is raised, the conditions become more oxidizing and the propensity for Ru to oxidize increases. Under reaction conditions at potentials of 0.3−0.7 V, the Pt surface atoms are present in the reduced state, while the Ru surface atoms are partially covered with hydroxyls, with the degree of coverage increasing with potential. The underlying (nonsurface) atoms may be either Pt or PtRu alloy, depending on how the catalyst is made and the prior history of the catalyst.

The results also indicate that the catalyst structure changes with operating conditions. While the rapid cycling and large voltage swings used in this study resulted in large driving forces for creating structural changes in the catalyst, slower changes may occur under actual operating conditions.

The results of this study do not support the recently proposed theory that ruthenium is present under reaction conditions as a bulk hydrous oxide, which acts as both a catalyst and a proton conductor, and that the way to enhance catalytic activity is to avoid PtRu alloy formation.[46,47] Those studies were based on ex-situ analysis of freshly prepared catalysts, and as the results here and in other studies[13,23] indicate, the catalysts change considerably under the more reducing potentials (0.3−0.6 V vs rhe) present during electrochemical methanol oxidation. In addition, bulk hydrous ruthenium oxide is not thermodynamically stable under the conditions where the reaction is typically carried out, even in the absence of reducing molecules such as methanol.[48] The application of higher electrode potentials than those commonly used for methanol oxidation (>0.7 V) may draw Ru atoms out of the bulk and lead to formation of bulk hydrous ruthenium oxides.

Several studies have debated the optimal Pt/Ru ratio for methanol oxidation catalysts. The solubility of Ru in the face-centered cubic Pt phase is about 60%,[7,49] and optimal catalyst compositions from Pt/Ru = 10:1[43] to Pt/Ru = 1:1[7] have been proposed. The results in this study indicated no loss in activity for methanol oxidation at 25 °C as the Ru was leached out of the sample with repeated cycling (Figure 12). However,

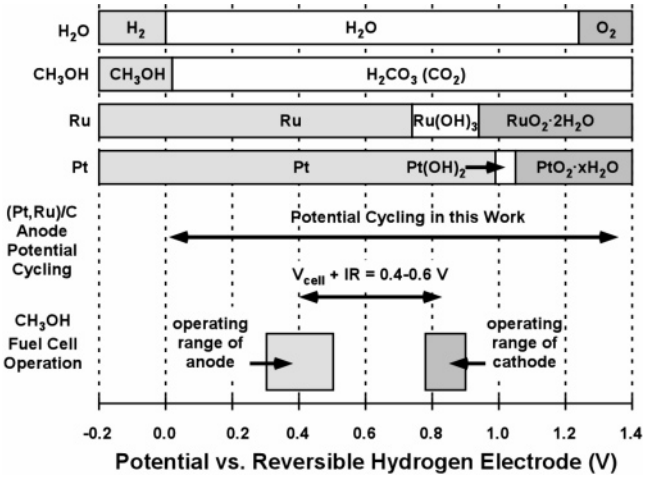

Figure 13. Stability of different materials in an acidic environment under standard conditions (pH = 0, hydrogen partial pressure = 1 atm) from data compiled by Porbeaux.[48] The range of potentials used during potential cycling in the present study is also shown, as well as the estimated range of anode and cathode potentials during operation of a direct methanol fuel cell.

additional studies have shown that anodes leached of Ru by repeated cycling perform much more poorly than fresh catalysts at 80 °C. The results are consistent with other work indicating that the optimal catalyst composition for high-temperature operation contains much higher Ru content than that for low-temperature operation.[2]

Metal Oxidation. The electrochemical oxidation of platinum in acidic electrolytes has been the topic of extensive study.[50,51] At standard conditions of pH = 0 and a hydrogen partial pressure of 100 kPa, metallic platinum is thermodynamically stable at low potentials. At a potential above about 0.98 V, $Pt(OH)_2$ is thermodynamically stable vs Pt. The electrochemical reaction relating these two phases is

$$Pt + 2H_2O = Pt(OH)_2 + 2H^+ + 2e^- \qquad (12)$$

At potentials above about 1.04 V, $PtO_2 \cdot 2H_2O$ becomes thermodynamically stable vs $Pt(OH)_2$. The stability regions for these three bulk Pt phases, based on the thermodynamic compilations of Pourbaix,[48] are shown in Figure 13.

Surface hydroxyl formation can occur on platinum surfaces at potentials well below those required for bulk oxidation. Hydroxyl formation becomes measurable in cyclic voltametry scans of Pt at room temperature above potentials of about 0.55 V.[50]

Similarly, metallic ruthenium oxidizes to $Ru(OH)_3$ at a potential of about 0.74 V through the reaction

$$Ru + 3H_2O = Ru(OH)_3 + 3H^+ + 3e^- \qquad (13)$$

$RuO_2 \cdot 2H_2O$ becomes thermodynamically stable vs $Ru(OH)_3$ at potentials above about 0.94 V. The stability regions for these three bulk phases are shown in Figure 13. In-situ XAS[22] and elliposometry[52] studies indicate that hydroxyl formation on ruthenium surfaces can be detected at potentials as low 0.25 V.

Methanol is a reducing agent and its presence decreases the propensity of Pt to oxidize at higher potentials. Balanced chemical reactions for the reduction of surface hydroxyls, Pt_s-OH, and bulk $Pt(OH)_2$ by methanol can be written as

$$6Pt_s-OH + CH_3OH = 6Pt_s + CO_2 + 5H_2O \qquad (14)$$

$$3Pt(OH)_2 + CH_3OH = 3Pt + CO_2 + 5H_2O \qquad (15)$$

These reactions do not result in current flow. Thus, electrochemical oxidation of Pt to $Pt(OH)_2$ by water competes with the chemical reduction of $Pt(OH)_2$ to Pt by methanol. The relative rates of these reactions determine whether Pt or $Pt(OH)_2$ is present during both steady-state and transient operating conditions. Mechanistically, the reductive capacity of methanol can be further understood by considering that each of the elementary steps involving hydrogen abstraction can be written as a combination of a chemical and an electrochemical step. For example, the first hydrogen abstraction can be written as

$$CH_3OH + 2Pt_s = Pt_s-CH_2OH + Pt-H \qquad (16)$$

$$Pt_s-H = Pt_s + H^+ + e^- \qquad (17)$$

Hydrogen chemisorbed on platinum can either undergo conversion to a proton followed by transport through the membrane or chemical reaction with surface hydroxyls to form water.

$$Pt_s-H + Pt_s-OH = 2Pt_s + H_2O \qquad (18)$$

By enhancing the rate of methanol oxidation, the presence of Ru on the surface of Pt creates an ample supply of chemisorbed hydrogen that helps keep the Pt component of the bifunctional catalyst in the reduced state at high potentials, conditions leading to oxidation and loss of activity for unalloyed Pt.

Metal Dissolution and Surface Compositional Changes. Cyclic voltametry in 0.5 M H_2SO_4 results in rapid, significant ruthenium loss from PtRu bimetallic catalysts. The slow dissolution of noble metals during cyclic voltametry in acidic solutions was studied by Rand et al.[53,54] Ruthenium was found to be particularly susceptible to dissolution, while the rate of platinum dissolution was low. The authors later reported the preferential dissolution of one element from several noble metal bimetallic alloys.[55] In an extensive study focused primarily on Rh loss from PtRh alloys during potential cycling at 100 °C in phosphoric acid, Mayell and Barber noted that Ru loss from PtRu alloys also took place under similar conditions.[56]

In this study, we observed that Ru dissolution also occurs in acidic media during potential cycling when methanol is present. We observed measurable ruthenium loss only when cycling between reduced and oxidized states of ruthenium. We observed no measurable ruthenium loss when the potential was cycled over narrower voltage ranges where Ru remained either fully reduced or oxidized.

Potential sweeps are often used in electrochemistry to clean Pt surfaces. Studies on bulk Pt surfaces demonstrate that repeated oxidation and reduction roughen Pt surfaces.[57] While no measurable Pt dissolution was observed during the short experiments in the present study, there is evidence that slow Pt dissolution may also occur when an electrode is repeatedly cycled between reducing and oxidizing states.[53,57]

In the present study, the catalyst activity for Pt/carbon increased during the first few potential cycles and the potential corresponding to Pt surface oxidation increased. The combination of both of these factors resulted in an increase in the peak methanol oxidation current. These results are attributed to changes in the supported Pt particles or their surfaces due to potential cycling.

Cyclic voltametry is a valuable tool for studying methanol oxidation catalysts.[50] Potential cycling following carbon monoxide chemisorption is also used to electrochemically measure the metal surface area and the activity of the catalyst for

electrochemical oxidation of chemisorbed CO.[31,33] The technique uses two potential cycles—the first to oxidize the CO, and the second to provide a baseline for differentiating the current due to CO oxidation from that due to other factors such as capacitive charging and metal oxidation. The work in this study indicates that the cyclic voltametry process itself changes the catalyst composition. Significant changes can occur in as few as one or two cycles, particularly for slow scan rates that extend to potentials up to 1.36 V.

Implications for Commercial Direct Methanol Fuel Cells. It is important to note that the experiments reported here were carried out under conditions that differ significantly from those used in actual fuel cells. The anode catalyst loadings used in this study were about an order of magnitude lower than those typically used for direct methanol fuel cells, resulting in current densities (expressed per unit of geometrical area) that are correspondingly about an order of magnitude lower. The studies here were carried out at 25 °C, while commercial direct methanol fuel cells are operated at temperatures of 40−100 °C, where turnover rates are 2−20 times higher. The experiments in this study were carried out under transient conditions, where the dependence of current density on potential is weaker than during steady-state operation. Even so, by comparison of the cyclic voltametry plots at 10 mV/s (Figures 3 and 6), the performance advantage of PtRu vs Pt of about 150−200 mV at the higher current densities is maintained.

During steady-state operation, direct methanol fuel cells are typically operated in the presence of a strong acidic solid electrolyte at anode overpotentials of about 0.3−0.5 V. These conditions correspond to potentials vs a standard hydrogen reference electrode that have about the same values. Thus, the steady-state potentials in DMFCs are more than 0.7 V lower than the peak potentials that the catalyst samples were exposed to in this study (Figure 13). Under these conditions, bulk Pt and Ru oxides, hydroxides, and hydrous oxides are not thermodynamically stable. Thus, ruthenium loss from PtRu alloys during steady-state DMFC operation is less likely to occur.

Ruthenium loss from DMFC anodes can occur if the fuel cell is operated in a manner that results in ruthenium oxidation and reduction. It has been suggested that deliberately increasing the anode potential to 1.0−1.2 V may restore anode potential lost during steady-state operation.[58] High anode potentials might also occur when the fuel cell is turned off due to slow oxygen diffusion from the cathode under open circuit conditions. Return to normal operating conditions with high methanol flow returns the catalyst to the reduced state. Both deliberate cycling of the anode to high potentials and repeated cycling between on and off states could eventually lead to significant ruthenium loss from the anode and a slow degradation in DMFC performance.

Conclusions

The use of X-ray absorption spectroscopy at constant photon energy in the near edge absorption region, when used in conjunction with known standards, is an easy method to follow transient phenomena that occur on a time frame of a few seconds to a few minutes. This work has demonstrated its utility for studying the catalyzed electrochemical oxidation of methanol during cyclic voltametry. The results emphasize the importance of in-situ studies for studying this reaction, which is carried out at potentials that lie intermediate between reducing and oxidizing conditions on small catalyst particles that typically contain 10−50% surface atoms. The nature of the catalyst surface changes as a function of potential, and these intermediate conditions are not readily duplicated ex situ in reducing (hydrogen), oxidizing (oxygen-containing) or inert (vacuum or nonreactive gas) environments.

The results of this work are consistent with a bifunctional catalyst mechanism for PtRu methanol electrooxidation catalysts. The presence of Ru has been shown to have a dramatic effect on keeping Pt reduced at high potentials in the presence of methanol. Repeated cycling between oxidizing and reducing conditions could eventually lead to significant ruthenium loss and loss of catalyst activity, suggesting that such conditions must be avoided for long catalyst life.

Acknowledgment. Use of the Advanced Photon Source was supported by the U.S. Department of Energy, Basic Energy Sciences, Office of Science, under Contract No. W-31-109-Eng-38. We thank W. M. Guise and D. A. Hancock for their experimental assistance. We also thank K. E. Schwiebert, S. Subramoney, C. A. Lundgren, L. Wang, D. T. Mah, S. Kumar, M. Abdou, and K. D. Kourtakis for fruitful discussions throughout the course of this work.

References and Notes

(1) Narayanan, S. R.; Valdez, T. I. In *Handbook of Fuel Cells − Fundamentals, Technology and Applications, Vol. 4: Fuel Cell Technology and Applications*; Vielstich, W., Gasteiger, H. A., Lamm, A., Eds.; John Wiley & Sons: Chichester, England, 2003; pp 1133−1141.

(2) Arico, A. S.; Srinivasan, S.; Antonucci, V. *Fuel Cells* **2001**, *1*, 133.

(3) Hamnett, A. In *Handbook of Fuel Cells − Fundamentals, Technology and Applications, Vol. 1: Fundamentals and Survey of Systems*; Vielstich, W., Gasteiger, H. A., Lamm, A., Eds.; John Wiley & Sons: Chichester, England, 2003; pp 305−322.

(4) Lamy, C.; Leger, J. M.; Srinivasen, S. In *Modern Aspects of Electrochemistry, Vol. 34*; Bockris, J. O. M., Conway, B. E., White, R. E., Eds.; Kluwer Academic/Plenum: New York, 2001; pp 53−118.

(5) McNicol, B. O.; Rand, D. A. J.; Williams, K. R. *J. Power Sources* **1999**, *83*, 15.

(6) Doyle, M.; Rajendran, G. In *Handbook of Fuel Cells − Fundamentals, Technology and Applications, Vol. 3: Fuel Cell Technology and Applications*; Vielstich, W.,Gasteiger, H. A., Lamm, A., Eds.; John Wiley & Sons: Chichester, England, 2003; pp 351−395.

(7) Watanabe, M.; Uchida, M.; Motoo, S. *J. Electroanal. Chem.* **1987**, *229*, 395.

(8) Prins, R. P.; Koningsberger, D. C. In *X-ray Absorption: Principles, Applications, Techniques of EXAFS, SEXAFS, and XANES*; Koningsberger, D. C., Prins, R., Eds.; John Wiley and Sons: New York, 1988; pp 321−372.

(9) Bart, J. C. J. *Adv. Catal.* **1986**, *34*, 203.

(10) Sinfelt, J. H.; Meitzner, G. D. *Acc. Chem. Res.* **1993**, *26*, 1.

(11) Clausen, B. S.; Topsoe, H.; Frahm, R. *Adv. Catal.* **1998**, *42*, 315.

(12) Allen, P. G.; Conradson, S. D.; Wilson, M. S.; Gottesfeld, S.; Raistrick, I. D.; Valerio, J.; Lovato, M. *Electrochim. Acta* **1994**, *39*, 2415.

(13) McBreen, J.; O'Grady, W. E.; Tourillon, G.; Dartyge, E.; Fontaine, A.; Pandya, K. I. *J. Phys. Chem.* **1989**, *93*, 6308.

(14) Weber, R. S.; Peuckert, M.; Dalla Beta, R. A.; Boudart, M. *J. Electrochem. Soc.* **1988**, *135*, 2525.

(15) Peuckert, M.; Yoneda, T.; Dalla Beta, R. A.; Boudart, M. *J. Electrochem. Soc.* **1986**, *133*, 944.

(16) Bregoli, L. J. *Electrochim. Acta* **1978**, *23*, 489.

(17) Blurton, K. F.; Greenberg, P.; Oswin, H. G.; Rutt, D. R. *J. Electrochem.* **1972**, *119*, 559.

(18) Abruna, H. D. In *Electrochemical Interfaces: Modern Techniques for In-Situ Interface Characterization*; Arubna, H. D., Ed.; VCH Verlag: Weinheim, Germany, 1991; pp 3−54.

(19) Adzic, R. R.; Wang, J. X.; Ocko, B. B. In *Handbook of Fuel Cells − Fundamentals, Technology and Applications, Vol. 2: Electrocatalysis*; Vielstich, W., Gasteiger, H. A., Lamm, A., Eds.; John Wiley & Sons: Chichester, England, 2003; pp 279−301.

(20) Lampitt, R. A.; Carrette, L. P. L.; Hogarth, M. P.; Russell, A. E. *J. Electroanal. Chem.* **1999**, *460*, 80.

(21) Russell, A. E.; Maniguet, S.; Matthew, R. J.; Yao, J.; Roberts, M. A.; Thompsett, D. *J. Power Sources* **2001**, *96*, 226.

(22) McBreen, J.; Mukerjee, S. J. *J. Electrochem. Soc.* **1995**, *142*, 23399.

(23) O'Grady, W. E.; Hagans, P. L.; Pandya, K. I.; Maricle, D. L. *Langmuir* **2001**, *17*, 3047.

(24) Bae, I. T.; Scherson, D. A. *J. Electrochem. Soc.* **1998**, *145*, 80.

(25) Radmilovic, V.; Gasteiger, H. A.; Ross, P. N. *J. Catal.* **1995**, *154*, 98.
(26) McKeown, D. A.; Hagans, P. L.; Carette, L. P. L.; Russell, A. E.; Swider, K. E.; Rolison, D. R. *J. Phys. Chem. B* **1999**, *103*, 4825.
(27) Dalla Betta, R. A.; Boudart, M.; Gallezot, P.; Weber, R. S. *J. Catal.* **1981**, *69*, 514.
(28) Gallezot, P.; Weber, R.; Dalla Beta, R. A.; Boudart, M. *Z. Naturforsch., A* **1979**, *34A*, 40.
(29) Lytle, F.; Wei, P. S. P.; Greegor, R. B.; Via, G. H.; Sinfelt, J. H. *J. Chem. Phys.* **1979**, *70*, 4849.
(30) Bae, I. T.; Scherson, D. A. *J. Phys. Chem.* **1996**, *100*, 19215.
(31) Dinh, H. N.; Ren, X.; Garzon, F. H.; Zelanay, P.; Gottesfeld, S. *J. Electroanal. Chem.* **2000**, *222*, 491.
(32) Boudart, M.; Djega-Mariadassou. G. *Kinetics of Heterogeneous Catalytic Reactions*; Princeton University Press: Princeton, NJ, 1984.
(33) Gasteiger, H. A.; Markovic, N.; Ross, P. N.; Cairns, E. J. *J. Phys. Chem.* **1994**, *98*, 617.
(34) Iwasita, T. In *Handbook of Fuel Cells − Fundamentals, Technology and Applications, Vol. 2: Electrocatalysis*; Vielstich, W., Gasteiger, H. A., Lamm, A., Eds.; John Wiley & Sons: Chichester, England, 2003; pp 603−624.
(35) Ross, P. N. In *Electrocatalysis*; Lipkowski, J., Ross, P. N., Eds.; Wiley-VCH: New York, 1998; pp 43−74.
(36) Wasmus, S.; Kuever, A. *J. Electroanal. Chem.* **1999**, *461*, 14.
(37) Parson, R.; VanderNoot, T. *J. Electroanal. Chem.* **1988**, *257*, 9.
(38) Markovic, N. M.; Ross, P. N. *Surf. Sci.Rep.* **2003**, *286*, 1.
(39) Jarvi, T. D.; Stuve, E. M. In *Electrocatalysis*; Lipkowski, J., Ross, P. N., Eds.; Wiley-VCH: New York, 1998; pp 75−153.
(40) Watanabe, M.; Motoo, S. *J. Electroanal. Chem.* **1975**, *60*, 267.
(41) Watanabe, M.; Suzuki, T.; Motoo, S. *Denki Kagaku* **1970**, *38*, 927.
(42) Krausa, M.; Vielstich, W. *J. Electroanal. Chem.* **1994**, *379*, 307.
(43) Gasteiger, H. A.; Markovic, N.; Ross, P. N.; Cairns, E. J. *J. Phys. Chem.* **1993**, *97*, 12020.
(44) Iwasita, T.; Hoster, H.; John-Anacker, A.; Lin, W. F.; Vielstich, W. *Langmuir* **2000**, *16*, 522.
(45) Dubua, L.; Coutanceau, C.; Garnier, E.; Leger, J.-M.; Lamy, C. *J. Appl. Electrochem.* **2003**, *33*, 419.
(46) Long, J. W.; Stroud, R. M.; Swider-Lyons, K. E.; Rolison, D. R. *J. Phys. Chem. B* **2000**, *104*, 9772.
(47) Rolison, D. R.; Hagans, P. L.; Swider, K. E.; Long, J. W. *Langmuir* **1999**, *15*, 774.
(48) Pourbaix, M. *Atlas of Elecrochemical Equilibria in Aqueous Solutions*; National Association of Corrosion Engineers: Houston, 1974.
(49) Hutchinson, J. M. *Platinum Metals Rev.* **1972**, *16*, 88.
(50) Vielstich, W. In *Handbook of Fuel Cells − Fundamentals, Technology and Applications, Vol. 2: Electrocatalysis*; Vielstich, W., Gasteiger, H. A., Lamm, A., Eds.; John Wiley & Sons: Chichester, England, 2003; pp 153−162.
(51) Jerkiewieca, G.; Tremiliosi-Filho, G.; Conway, B. E. *J. Electroanal. Chem.* **1992**, *334*, 359.
(52) Ticanelli, E.; Beery, J. G.; Paffett, M. T.; Gottesfeld, S. *J. Electroanal. Chem.* **1989**, *258*, 61.
(53) Rand, D. A. J.; Woods, R. *J. Electroanal. Chem.* **1972**, *35*, 209.
(54) Mitchell, D.; Rand, D. A. J.; Woods, R. *J. Electroanal. Chem. Interfacial Electrochem.* **1978**, *89*, 11.
(55) Rand, D. A. J.; Woods, R. *Electroanal. Chem.* **1972**, *36*, 57.
(56) Mayell, J. S.; Barber, W. A. *J. Electrochem. Soc.* **1969**, *116*, 1333.
(57) Biegler, T. *J. Electrochem. Soc.* **1969**, *116*, 1131.
(58) Hoster, H.; Iwasita, T.; Baumgaertner, H.; Vielstich, W. *J. Electrochem. Soc.* **2001**, *148*, A496.